Influenza A Virus Compromises anti-Streptococcal Innate Immunity

Johann Volzke[1,*], Maria Brendel[1], Erik Weipert[1], Michael Müller[1], Daniel Schultz[2], Ko-Infekt Study Group[2,3,4] , Brigitte Müller-Hilke[1]

[1]Core Facility for Cell Sorting and Cell Analysis, Rostock University Medical Center, Rostock, Germany

[2]Institute of Biochemistry, University of Greifswald, Greifswald, Germany

[3]Institute of Immunology, Friedrich-Loeffler-Institut, Greifswald-Insel Riems, Germany

[4]Institute of Medical Microbiology, Virology and Hygiene, Rostock University Medical Center, Rostock, Germany

*Correspondence: johann.volzke@med.uni-rostock.de

Abstract

Seasonal influenza epidemics pose a considerable hazard for global health. In the past decades, accumulating evidence revealed that influenza A virus (IAV) renders the host vulnerable to bacterial superinfections which in turn are a major cause for morbidity and mortality. However, whether the impact of influenza on anti-bacterial innate immunity is restricted to the vicinity of the lung or systemically extends to remote sites is underexplored. We therefore sought to investigate intranasal infection of adult C57BL/6J mice with IAV H1N1 in combination with bacteremia elicited by intravenous application of Group A Streptococcus (GAS). Co-infection *in vivo* was supplemented *in vitro* by challenging murine bone marrow derived macrophages and exploring gene expression and cytokine secretion. Our results show that viral infection of mice caused mild disease, led to persistent pulmonary immune response in the lung and induced the depletion of CCL2 in the periphery. Influenza preceding GAS infection promoted the unopposed dissemination of bacteria and their invasion into remote tissues like lung and joints and was accompanied by exacerbated sepsis. *In vitro* co-infection of macrophages led to significantly elevated expression of TLR2 and CD80 compared to bacterial mono-infection, whereas CD163 and CD206 were downregulated. The GAS-inducible upregulation of inflammatory genes, such as *Nos2*, as well as the secretion of TNFα and IL-1β were notably reduced or even abrogated following co-infection. Our results indicate that IAV primes an innate immune layout that is inadequately equipped for bacterial clearance.

keywords: influenza A virus, Group A Streptococcus, co-infection, inflammation, sepsis, macrophage, innate immunity

33 # 1 Introduction

34 Seasonal influenza is a major cause of respiratory disease that affects 5 – 10% of the global
35 population annually with an estimated death toll of up to 500,000 [1,2]. The segmented genome
36 of influenza A virus (IAV) combined with an error-prone RNA polymerase enables the periodical
37 emergence of new strains with elevated pandemic capacities, which annually challenge
38 humankind yet devoid of adequate adaptive immunity [3,4]. The most prominent paradigm for
39 the dramatic consequences of an influenza pandemic is the 1918/1919 flu that caused roughly 50
40 Million casualties [5]. Notably, the vast majority of fatal cases were attributed to secondary
41 bacterial infections predominantly caused by pneumococci and hemolytic streptococci [6,7].
42 Along these lines, excess morbidity due to bacterial superinfection with the nasopharyngeal
43 colonizers *S. pneumoniae*, *S. aureus* and *S. pyogenes* (Group A Streptococcus, GAS) was
44 confirmed for the most recent influenza pandemic in 2009 [8]. As of yet, there is neither a
45 licensed vaccine against S. *aureus* nor against *S. pyogenes* that would help contain invasive
46 infections with these pathogens during future influenza pandemics [9–11].

47 Several modes by which an immune response against IAV supports viral clearance yet fails
48 to oppose bacterial pathogens have been suggested [1]. For instance, Okamoto and colleagues
49 demonstrated that IAV infection led to the presentation of hemagglutinin (HA) by epithelial cells,
50 which is utilized by GAS to breach cellular barriers [12,13]. Other groups reported that HA,
51 among other viral proteins, caused the exposure of receptors that act as adhesins for bacterial
52 attachment and invasion [14–16]. Others showed that viral infection caused damage of the
53 respiratory epithelium, expediting initial bacterial adherence [6,17,18]. Moreover, experimental
54 data indicated that IAV paves the way for the dissemination of opportunistic bacterial pathogens
55 by impacting the innate immune response, which is critical for bacterial containment [19,20]. In
56 fact, the virus was shown to induce an increased secretion of anti-inflammatory interleukin (IL-

57)10 as well as inflammatory type I and type II interferons (IFNs), which was associated with
58 both, impaired phagocytic activity by pulmonary immune cells and diminished production of
59 chemokines [14,19,21–24].

60 Together, these data illustrate some aspects of post-influenza pneumonia and the interplay
61 of viral and bacterial pneumopathogens in life-threatening infections. While the aforementioned
62 studies focused on bacterial superinfections of the respiratory tract, we were intrigued by the fact
63 that influenza outbreaks regularly coincide with a broad spectrum of invasive infectious diseases
64 like necrotizing fasciitis, septic arthritis and bacteremia associated with GAS [8,25–27]. We
65 therefore asked whether pulmonary IAV can also alter systemic innate immunity and facilitate
66 secondary bacterial insults at remote sites. We were particularly interested in the impact IAV
67 exerts on the response of macrophages – immune cells that are indispensable for initial anti-
68 streptococcal resistance [19,28,29]. We established co-infection models that *in vivo* combined
69 respiratory IAV infection with GAS bacteremia and *in vitro* investigated primary macrophages
70 for their potential to respond to both pathogens simultaneously.

71 # 2 Materials and Methods

72 ## *2.1 Pathogens*

73 Pandemic influenza A virus (IAV) A/Germany-BY/74/2009 (H1N1pdm09) propagation
74 and titer determination was performed as previously described [30]. In brief, IAV was replicated
75 in Mardin-Darby canine kidney II (MDCKII) cells using minimal essential medium
76 supplemented with 0.2% bovine serum albumin and 2 µg/mL N-Tosyl-L-phenylalanin-
77 chlormethylketon (Sigma). For the determination of the tissue culture infectious dose 50
78 ($TCID_{50}$), virus suspensions were serially diluted and applied to MDCKII cultures. Cells were
79 then incubated for three days at 37°C and 5% CO_2 followed by examination of cytopathogenicity.

80 *Streptococcus pyogenes* (Group A Streptococcus, GAS) strain AP1 of the *emm1* (M1)
81 serotype was originally acquired from the World Health Organization Collaborating Center for
82 Reference and Research on Streptococci (Prague, Czech Republic). Bacteria were thawed onto
83 Colombia agar plates containing 5% sheep blood (Becton Dickinson) and were cultured
84 overnight followed by storage at 4°C for up to three weeks. Colonies were picked from the plate,
85 suspended into Todd-Hewitt broth (THB, Becton Dickinson) and cultured overnight at 37°C and
86 5% CO_2. The suspension was diluted 20-fold in THB and bacteria were incubated until
87 exponential phase of growth was reached. Subsequently, bacteria where washed thrice with PBS
88 (Thermo Fisher) prior to their application in mice and *in vitro* infection models, respectively. The
89 determination of colony forming units (CFU) was performed the following day by counting of
90 serially diluted suspensions.

91 ## *2.2 Animals*

92 C57BL/6J mice were initially purchased from Charles River. Mice were bred in the animal
93 core facility under specific germ-free conditions. Animals were transferred to individually
94 ventilated cages prior to infection experiments and were housed at a 12-hour light/dark cycle, an

95 ambient temperature of 22 ± 2°C and 50 ± 20% humidity. Food and water were provided *ad*
96 *libitum*. Animal experiments were reviewed and approved by the ethics committee of the State
97 Department for Agriculture, Food Safety and Fishery in Mecklenburg-Western Pomerania under
98 the file reference number 7221.3-1-017/19.
99
100 *2.3 In vivo infection models and clinical scoring*
101 For the induction of viral infections, 20 µL of a suspension containing 1.5×10^5 $TCID_{50}$
102 IAV were applied to both nostrils of 20- to 22-week old male mice under anesthesia by isoflurane
103 inhalation. This volume was chosen in order to guarantee an infection of both, the upper and
104 lower respiratory tracts [31]. Applying the same volume of PBS only served as the negative
105 (healthy) control. Mice were subsequently monitored daily for 16 days for alterations in body
106 weight relative to the day of infection (day 0). On days 2, 4 and 7, a maximum of 80 µL of anti-
107 coagulated blood was drawn by saphenous venipuncture using a 25G needle followed by
108 centrifugation and collection of plasma. On day 16, mice were anesthetized with 75 mg of
109 Ketamine (Pharmanovo) and 5 mg Xylazin (Bayer) per kg bodyweight. Subsequently, mice were
110 exsanguinated by cardiac puncture. Mice were then sacrificed by cervical dislocation and lungs
111 were excised, snap frozen and stored at -80°C for later analyses.
112 In order to induce bacteremia, GAS was diluted in PBS and 1×10^5 CFU were applied by
113 injection into the lateral tail vein. Intravenous injection of PBS served as a control. For co-
114 infection, IAV was applied as described above either two days prior or subsequent to bacterial
115 infection. Mice were given tramadol (Ratiopharm) in drinking water for analgesia. Animals were
116 monitored following bacterial infection for a maximum of 14 days or until humane endpoints
117 were reached. Sepsis severity was assessed by a scoring system that incorporated the assessment
118 of macroscopic signs of burden as previously described [32,33]. In brief, scores of four categories

119 were added together to provide an estimate for overall sepsis activity: i) weight loss of ≥ 5%
120 (Score 5), ≥ 10% (Score 10), ≥ 20% (Score 20, humane endpoint); ii) appearance deviations such
121 as piloerection (Score 5), high myotonicity or scruffy orifices (Score 10), convulsions or paralysis
122 (Score 20, humane endpoint); iii) impairment of consciousness such as suppressed activity or
123 limited reaction to stimuli (Score 5), self-isolation or lethargy (Score 10), perpetual pain
124 vocalization or apathy (Score 20, humane endpoint) and iv) signs of impaired respiratory quality
125 or inflammation such as edemas on small body areas (Score 5), disseminated edemas or labored
126 breathing (Score 10), open wounds or gasping (Score 20, humane endpoint).

127 Mice were sacrificed as described above upon reaching the end of the observation period, at
128 any humane endpoint or when reaching an overall sepsis score of ≥ 20. Cardiac blood samples
129 were plated on blood agar and medial arthrotomy on both knee joints was performed under a
130 stereo microscope followed by plating of the synovial fluid on blood agar. Agar plates were
131 subsequently incubated overnight and examined for the presence of β-hemolytic bacteria. Hind
132 paws were extracted, snap frozen and stored at -80°C for the analysis of eicosanoids.

133

134 *2.4 Eicosanoid extraction and analysis*

135 Lipidomics analyses were performed as previously described [32]. In brief, paw samples
136 were chilled in liquid nitrogen, pulverized and 50 mg of the resulting powder was immersed in
137 500 µL cold methanol containing 0.1% butylated hydroxytoluene and 500 µL ice cold water. 100
138 µL deuterated internal standards containing 12-HETE-d_8, 13-HODE-d_4, PGE_2-d_4 and Resolvin
139 D1-d_5 (each 100 ng/mL, Cayman Chemicals) were subsequently added followed by an additional
140 lysis step with matrix B at 6 m/s for 45 s on a FastPrep (MP Biomedicals). Following this, 300
141 µL sodium acetate (1 M) was added on ice and 10 M acetic acid was added until pH 6 was
142 reached. Solid phase extraction was performed on methanol and sodium acetate conditioned

143 Bond Elut Certify II cartridges (Agilent). After loading the samples, cartridges were washed with
144 50% methanol. Elution of eicosanoids was carried out by addition of hexane/ethyl acetate (75/25)
145 containing 1% acetic acid.

146 For measurements, paw extracts were dried under nitrogen flow using a TurboVap
147 (Biotage) and reconstituted in 70 µL 25% acetonitrile. Separation was done on a Gemini NX-C18
148 column (3 µm, 100 × 2 mm) utilizing an Agilent 1200 series HPLC systems. Dynamics multiple
149 reaction monitoring MS/MS was executed using a 6460 series triple quadrupole tandem mass
150 spectrometer (Agilent) with electrospray ionization in negative mode. Calibration by internal and
151 external standards was performed as previously described [32]. Agilent Mass Hunter Qualitative
152 Analysis software and Agilent Mass Hunter Quantitative Analysis software (both version
153 B.07.00) were used for MS data analysis. Quantities of individual eicosanoids were standardized
154 to a mean of 0 and a standard deviation of 1 for data visualization.

155

156 *2.5 Isolation of RNA and DNA from lung samples*

157 Lung samples were submerged in liquid nitrogen, slightly fragmented and weighed. Sixty
158 to one hundred twenty milligrams were transferred to lysis tubes containing bashing beads (Zymo
159 Research) and 1 mL TRIzol (Thermo Fisher). Lung fragments were subsequently homogenized at
160 4,000 rpm for 4 × 20 s using a FastPrep. Samples were then centrifuged at 10,000 × *g* for 7 min at
161 4°C and transferred into new tubes. Apart from centrifugation at 4°C, the following steps were
162 conducted at room temperature. After resting for 5 min, 200 µL chloroform (Sigma) was added
163 and samples were extracted for 3 min. Subsequently, samples were centrifuged for 15 min at
164 12,000 × *g*. The RNA-enriched upper phase was mixed with 500 µL 2-propanol, incubated for 10
165 min and centrifuged at 12,000 × *g* for 10 min. RNA pellets were suspended in 75% Ethanol
166 followed by centrifugation at 7,500 × *g* for 5 min. Supernatants were subsequently discarded,

167 pellets were dried and dissolved in 40 µL RNAse-free water by incubation at 60°C for 15 min.
168 RNA contents were then determined photometrically on a NanoDrop (Thermo Fisher). DNA was
169 isolated by precipitation of the appropriate phase upon addition of 300 µL ethanol, incubation for
170 3 min and centrifugation for 5 min at 2,000 × *g*. The resulting pellet was then washed twice by 30
171 min incubation with 0.1 M sodium citrate (pH 8.5) in 10% ethanol. DNA samples were
172 subsequently suspended in 75% ethanol and incubated for 20 min. After centrifugation,
173 supernatants were discarded, pellets were dried and dissolved by incubation in 8 mM NaOH for
174 10 min. DNA contents were determined fluorometrically using the Qubit 1X dsDNA Assay Kit to
175 the manufacturer's instructions (Thermo Fisher).
176
177 *2.6 Lung pathogen burden and gene expression*
178 Primer pairs were designed for the detection of IAV H1N1 matrix protein, nucleoprotein
179 and hemagglutinin in murine lung extracts according to the strain specific sequences found at
180 https://www.fludb.org/brc/fluStrainDetails.spg?strainName=A%2FGermany-
181 BY%2F74%2F2009%28H1N1%29&decorator=influenza (supplementary Table I). For this,
182 RNA was isolated as described above and 500 ng were reverse transcribed using the High
183 Capacity cDNA Reverse Transcription Kit (Thermo Fisher) according to the manufacturer's
184 instructions. Twenty-five nanograms of the resulting cDNA together with 500 nM of the primer
185 pairs were submitted to qPCR using the PowerUP SYBR Green Mastermix (Thermo Fisher). The
186 amplification reaction was monitored on the ViiA 7 Real-Time PCR System running on the
187 QuantStudio Real Time PCR Software V1.3 (Thermo Fisher). The size of the respective
188 amplicons was confirmed by 2% agarose gel and ethidium bromide staining. Primer pairs for the
189 detection of GAS strain AP1 specific genomic DNA were designed according to sequence
190 information found at https://www.ncbi.nlm.nih.gov/nuccore/CP007537?report=genbank

191 (supplementary Table II). A total of 20 ng DNA from lung extracts were used together with 500
192 nM of the primer pairs for qPCR as described above, followed by confirmation of amplicon sizes
193 on agarose gels. Gene expression analyses were performed on 25 ng cDNA that was obtained
194 from reverse transcribed lung RNA. For qPCR analysis, TaqMan primer pairs and probes
195 (Thremo Fisher) were used for *Ccl2* (assay ID: Mm00441242_m1) and *Ifnb1* (Mm00439552_s1)
196 utilizing *Gapdh* (Mm05724508_g1) as a reference gene. All reactions were amplified using the
197 TaqMan Gene Expression Master Mix (Thermo Fisher).
198
199 *2.7 Bone marrow derived macrophage infection model*

200 C57BL/6J mice used for bone marrow isolation had a median age of 10 weeks (range 7 –
201 42 weeks) and 30% were female. Bone marrow was obtained from long bones by centrifugation
202 as previously described [34]. The resulting pellet was subsequently suspended in Dulbecco's
203 Modified Eagle's Medium (DMEM) supplemented with 10% fetal calf serum (FCS), 5 IE/mL
204 Penicillin, 5 µg/mL Streptomycin, 2 mM L-Glutamine (Thermo Fisher), 10 mM HEPES and 1
205 mM sodium pyruvate (PAN Biotech). After determination of vital cells using a hemocytometer
206 and trypan blue (Thermo Fisher), cells were seeded into 6-well culture plates (Greiner) at a
207 density of 3×10^5 cells per cm^2 in 2 – 5 mL supplemented DMEM. The differentiation to
208 macrophages was initiated at day 0 by the addition of 20 ng/mL macrophage colony-stimulating
209 factor (M-CSF, R&D Systems). Cells were cultured afterwards at 37°C and 5% CO_2 for 7 days
210 including the replacement of supplemented DMEM and replenishment of M-CSF at days 1 and 4.
211 For viral infection (day 7, t_0), supplemented DMEM was refreshed and 4×10^5 $TCID_{50}$ IAV were
212 added. Following this, infected or uninfected macrophages were incubated for 48 h upon which
213 the cells were either collected for downstream analyses or submitted to bacterial (super-)infection
214 (day 9). In case of the latter, supplemented DMEM was removed, the cells were washed thrice

215 with PBS and Minimal Essential Medium α containing additional nucleosides and 10% FCS
216 (Thermo Fisher) was added. GAS was then applied at 4.5 × 10^6 CFU. Subsequently,
217 macrophages were incubated for 6 h followed by sample collection.
218
219 *2.8 Single cell analysis by flow cytometry*
220 Gentle detachment of macrophages from culture plates was carried out by washing with
221 PBS and subsequently incubating with 5 mL PBS containing 10 mM EDTA for 10 min. Culture
222 plates were tapped multiple times and suspensions were collected afterwards. For increased
223 yields, 0.7 mL accutase (Pan Biotech) was added for 10 – 15 min followed by alternately tapping
224 and pipetting. Subsequently, another 0.7 mL accutase were added for an additional 10 – 15 min,
225 tapping and pipetting were repeated and suspensions collected and pooled with the PBS/EDTA
226 fraction. Finally, 1 mL supplemented DMEM was added and the remaining cells were obtained
227 using a cell scraper (Sarstedt). Suspensions were centrifuged at 400 × *g* and 4°C for 5 min and
228 cells were suspended in autoMACS Running Buffer (RB, Miltenyi Biotec) followed by counting.
229 Antibody binding to CD16 and CD32 was prevented by incubation of macrophages with 0.5 µg
230 Trustain FcX (Biolegend) in RB supplemented with 10% FCS for 10 min on ice. Subsequently,
231 an antibody mixture containing 0.13 µg (anti-)F4/80:FITC (clone BM8), 0.5 µg CD163:APC
232 (S150491), 0.25 µg CD206:BV605 (C068C2), 0.25 µg CD80:BV421 (16-10A1, Biolegend), 0.22
233 µg CD86:APC/Vio770 (PO3.3), 4.5 µL TLR2:PE (REA109) and 0.15 µg MHCII:PerCP/Vio770
234 (REA813, Miltenyi Biotec) was added and incubated for 20 min on ice in the dark. Cells were
235 washed afterwards, suspended in RB and 7-Aminoactinomycin (7-AAD, Biolegend) was added at
236 a concentration of 1.25 µg/mL for at least 5 min prior to measurement.
237 Data acquisition was performed on the Aurora spectral flow cytometer running on the
238 SpectroFlo software v2.2.0.3 (Cytek Biosciences). Data analysis was conducted using the FlowJo

239 software v10.7.1. Supplementary Fig. 1 illustrates the gating strategy. Live macrophages were
240 identified as 7-AAD^{-}F4/80^{+} singlets. This population was used for the subsequent determination
241 of expression levels based on median fluorescence intensity (MFI) values and as a parent for
242 measuring the proportions of subpopulations expressing different combination of the above-listed
243 surface antigens. For dimension reduction, 10,000 macrophage events were down-sampled,
244 concatenated and submitted to the algorithm t-distributed stochastic neighbor embedding (t-SNE)
245 using an automated learning configuration (opt-SNE combined with the exact KNN algorithm
246 and the Barnes-Hut gradient algorithm) with a perplexity of 50 and a maximum of 1000 iterations
247 [35]. Unsupervised clustering of subpopulations expressing any combinations of the analyzed
248 surface proteins was conducted by FlowSOM [36].
249
250 *2.9 Macrophage gene expression*
251 After aspirating cell culture supernatants, 700 µL of a chaotropic agent solution (Qiagen)
252 was added to individual wells and cells were lysed by scraping and vigorous shaking. RNA was
253 subsequently isolated using the RNeasy Plus Mini Kit (Qiagen) after the manufacturer's
254 instructions. Quantification of RNA contents were determined photometrically and 200 ng RNA
255 was submitted to reverse transcription as described above. Amplification of cDNA was then
256 performed by TaqMan Gene Expression Master Mix, primer pairs and probes for the relative
257 quantification of *Ccl2*, *Cxcl2* (assay ID: Mm00436450_m1), *Ifnb1*, *Il1b* (Mm00434228_m1), *Il6*
258 (Mm00446190_m1), *Il10* (Mm00439614_m1), *Mgl2* (Mm00460844_m1), *Nos2*
259 (Mm00440502_m1), *Tgfb1* (Mm01178820_m1) and *Tnf* (Mm00443258_m1) using *Gapdh* as a
260 reference gene. Polymerase chain reactions were performed on the Viia 7 System. In detail,
261 samples were first incubated for 2 min at 50°C followed by 10 min at 95°C for polymerase
262 activation. Subsequently, 40 automated cycles of PCR were performed that incorporated

263 denaturation at 95°C for 15 sec and annealing and elongation at 60°C for 1 min. After each cycle
264 the fluorescein amidite fluorescence signal was measured. Ct values were obtained when
265 fluorescence intensities reached data-dependent and automatically defined thresholds.
266 Quantification of gene expression was then performed by the $2^{-\Delta\Delta Ct}$ Method that incorporated
267 normalization of the target gene Ct values to the reference gene (ΔCt) as well the difference
268 between ΔCt values from uninfected and infected cells (ΔΔCt).
269
270 *2.10 Cytokine analysis*
271 Cytokine concentration in mouse plasma samples were quantified by a 3-plex
272 LEGENDplex assay (Biolegend) that contained capture beads and detection antibodies for CCL2
273 (monocyte chemoattractant protein-1, MCP1), Interferon (IFN)γ and tumor necrosis factor
274 (TNF)α. For the quantification of CCL2, Interleukin (IL-)1β, IL-6, IL-10 and TNFα in cell
275 culture supernatants, a 5-plex LEGENDplex assay was used following the manufacturer's
276 guidelines. Data acquisition was performed on the Cytek Aurora flow cytometer. Cell culture
277 supernatant concentrations of CXCL2 (macrophage inflammatory protein 2-α, MIP2-α) were
278 determined by the CXCL2/MIP-2 DuoSet enzyme linked immunosorbent assay (ELISA) kit to
279 the manufacturer's instructions (R&D Systems). Horseradish peroxidase-catalyzed color reaction
280 were initiated by addition of the TMB Substrate Kit (Biolegend) and quenched by 0.5 M sulfuric
281 acid (Merck). The absorbance at 450 nm was measured on the Infinite M200 spectral photometer
282 (Tecan).
283
284 *2.11 Statistical analysis*
285 Data analysis and visualization were performed using RStudio v1.2.5033 that ran R v3.5.1.
286 Normalization was either performed by division of individual values from infection groups and

control groups, respectively, or by feature scaling into a 0 – 1 range by the formula $x_i' = (x_i - x_{min})/(x_{max} - x_{min})$. Heatmaps and hierarchical clusters were generated with the "pheatmap" package that incorporated feature scaling by standardization applying the formula $z_i = (x_i - \bar{x})/\sigma$. Calibration curves were fitted and samples values were estimated by n-parameter logistic regression using the "nplr" package. Two-sided statistical tests were used for the comparisons of group medians or means. Repeated measures (body weight trajectories) were compared by one-way and two-way analyses of variance (ANOVA), respectively. Probabilities of survival and incidences were compared by the logrank test. Bivariate interdependencies were evaluated by the Pearson product-moment correlation coefficient (r). Data sets were tested for normality by the Shapiro-Wilk test. Normal distribution of within-group raw or normalized variables was rejected when the test resulted in a p-value of < 0.05. Depending on the outcome of this test, univariate statistical analyses on variables that were normalized to respective controls were performed by the one-sample Wilcoxon signed rank test and the one-sample t-test, respectively. Two independent samples were compared with the Mann-Whitney U test or the t-test. Comparisons of variables between multiple groups were performed with the Dunn's test and the Tukey HSD test, respectively, in combination with type I error correction using the Bonferroni-Holm method. A p-value of < 0.05 was considered statistically significant.

304 # 3 Results

305 ## *3.1 Infection with influenza A virus H1N1 caused mild symptoms and induced a persistent*
306 *immune reaction in the lung*

307 In order to examine clinical manifestations of influenza, we used a model of intranasal
308 infection with 2009 pandemic H1N1 IAV in adult mice (Fig. 1A). Intranasal application of PBS
309 served as a control. Mice were monitored for relative weight loss post infection as a proxy for
310 disease severity and indeed, exhibited minor reductions in body weight as early as two days after
311 virus application (Fig. 1B). This trend continued until day seven after infection and resulted in a
312 maximum weight loss of 5.5% ± 2.1% (mean ± SEM). Thereafter, body weight continuously
313 increased and returned to starting values by day 14 suggesting robust recovery from infection.
314 When comparing weight trajectories over the entire observation period using two-way analysis of
315 variance (ANOVA), we found a statistically significant difference between infected mice and
316 uninfected controls ($p < 0.001$). In accordance with the observed mild disease courses, we did not
317 measure quantifiable amounts of the inflammatory cytokines TNFα and IFNγ in plasma samples
318 from IAV infected animals (not shown). We did, however detect significant reductions of plasma
319 CCL2 concentrations by 12.8% and 13.6% at days two and four after infection, respectively,
320 relative to uninfected controls (Fig. 1C). By day seven, CCL2 plasma levels equalized between
321 both groups ($p = 0.65$, not shown).

322 In order to examine immune responses in the lower respiratory tract, we further performed
323 gene expression analyses on whole lung homogenates that were obtained 16 days after IAV
324 application. For this, we focused on mRNA expression levels of *Ccl2* and *Ifnb1*, as the former
325 was altered in the periphery and the latter can be indicative of an anti-viral response. Protein data
326 were not collected because of limited sample quantities. We found no meaningful differences in
327 the expression of *Ccl2* between the IAV and control groups (Fig. 1D, left panel). Interestingly,

328 *Ifnb1* expression was found to be significantly increased in lungs from infected mice (Fig. 1D,
329 right panel). Given this prolonged immune activation, we consequently utilized primer pairs for
330 the detection of viral genes in lung samples that code for hemagglutinin, matrix protein and
331 nucleoprotein (supplementary Fig. 2). We indeed detected IAV specific RNA in 38% (3/8) of
332 infected animals by quantitative PCR (Fig. 1E). False positive detection of unspecific targets was
333 ruled out by confirming the expected amplicon melting temperatures (supplementary Fig. 3).
334 However, the quantities of all three viral genes were generally low ($C_t > 32$) and might rather
335 indicate residual viral antigen.

336 In summary, we here show that an infection with IAV H1N1 in mice induced minor clinical
337 manifestations that were accompanied by reductions of plasma CCL2 levels. Our data further
338 show that residual genetic material of the virus persisted in the lungs, which was accompanied by
339 an ongoing type I IFN immune response.

340

341 *3.2 Group A Streptococcal sepsis was aggravated following Influenza A virus infection*

342 As CCL2 is integral to bacterial control yet reduced during respiratory tract infection with
343 IAV, we sought to investigate the clinical features of IAV superimposed bacteremia. To this end,
344 we compared infection with bacteria only to co-infection models combining intranasal virus
345 application with intravenous GAS infection in alternating succession (Fig. 2A). By monitoring
346 for macroscopic symptoms following bacterial infection, we observed the occurrence of localized
347 paw inflammation (Fig. 2B). Of note, the emergence of these edemas was accelerated and more
348 frequent in post-influenza bacteremia (IAV+GAS) compared to bacterial infection only (GAS, p
349 = 0.01) and pre-influenza bacteremia (GAS+IAV, p = 0.045), respectively (Fig. 2C). In detail,
350 80% (8/10) of mice in the IAV+GAS group exhibited signs of paw inflammation already one day
351 after bacterial infection. In contrast, the incidence of paw edemas was increased to only 40%

352 (4/10) in the GAS+IAV group as opposed to 20% (2/10) in the GAS only group, and this
353 difference did not reach statistical significance (p = 0.33). We further analyzed eicosanoids from
354 paw extracts and found that these immunologically active lipid metabolites were upregulated in
355 some animals irrespective of the (co-)infection regimen (supplementary Fig. 4).

356 Additionally, more blood smears and knee joint capsule swabs were positive for β-
357 hemolytic bacteria in co-infected mice from the IAV+GAS group (Table I), which suggested that
358 preceding influenza promoted bacterial dissemination and invasion into synovial tissues. By
359 assessing macroscopic signs of burden as a proxy for sepsis severity (see Materials and Methods),
360 we found a significantly increased median disease score when comparing post-influenza
361 bacteremia with monocausal GAS infection (Fig. 2D). Interestingly, when correlating sepsis
362 scores with eicosanoids from paw homogenates, we found a significant relationship between the
363 individual disease severity and the corresponding amounts of prostaglandins D_2 and E_2 as well as
364 5- and 12-Hydroxyeicosatetraenoic acid (supplementary Table III). Furthermore, elevated disease
365 severity in the IAV+GAS group was paralleled by a reduction in survival probability to 40%
366 compared to 80% in the GAS only group (Fig. 2E). In contrast, mice from the GAS+IAV group
367 had an only marginally decreased survival chance of 70%. However, the overall probability for a
368 fatal outcome was, according to logrank statistics, not significantly different between groups (p =
369 0.13) and this was likely due to low sample sizes and a high degree of uncertainty.

370 For our further analyses, we focused on the IAV+GAS co-infection sequence because our
371 data suggested that the clinical outcome was not different between the GAS+IAV and GAS
372 groups. We next aimed to investigate whether post-influenza GAS infection impacted on the
373 immune activation in the lower respiratory tract. To this extent, we analyzed lung homogenates
374 for the expression of *Ccl2* and *Ifnb1*, and compared the data from co-infected mice to GAS
375 mono-infection or uninfected controls. We found that neither GAS nor IAV+GAS infection

376 resulted in a meaningful alteration of the *Ccl2* expression in the lung (Fig. 2F, left panel). Of
377 note, lungs from both mono- and co-infected mice exhibited a median 2-fold upregulation of
378 *Ifnb1* relative to lungs from uninfected animals ($p = 0.008$ for GAS and $p = 0.039$ for IAV+GAS;
379 Fig. 2F, right panel). Yet, when comparing the infection regimens with each other, we found that
380 *Ifnb1* overexpression was comparable between both infection groups ($p = 0.93$).We were curious
381 whether the bacteria are capable of disseminating from the blood into the lower respiratory tract
382 and therefore analyzed lung homogenates for the presence of GAS specific genes using
383 quantitative PCR (supplementary Fig. 5). Indeed, we detected genomic speB in four out of nine
384 lungs from the IAV+GAS group whereas only one out of nine lungs from the GAS group was
385 positive for this bacterial gene (Fig. 2G, left panel). However, when analyzing for spy2158, only
386 two lung extracts from the IAV+GAS group were positive (Fig. 2G, right panel). Specific
387 amplification was again confirmed by melting curves (supplementary Fig. 6). As whole lungs
388 were submitted to chaotropic agent assisted homogenization and PCR analysis, we were not able
389 to confirm whether there were any vital bacteria present in these samples.

390 Collectively, our *in vivo* data demonstrated that a preceding IAV infection of the respiratory
391 tract aggravated bacteremia by promoting bacterial dissemination into remote tissues, localized
392 inflammation and a dysregulated host response as shown by an elevated sepsis activity. In
393 contrast, application of the virus following an already established bacteremia did not influence
394 disease progression and outcome.

395

396 *3.3 Preceding influenza A virus infection impacted on the Group A Streptococcus induced*
397 *diversification of macrophage surface expression profiles*

398 As our *in vivo* co-infection model implicated a preceding IAV infection to cause impaired
399 control of the bacterial burden following a superimposed GAS infection, we sought to explore

400 any modification of anti-bacterial innate immunity. To this end, we chose *in vitro* (co-)infection
401 models of primary macrophages. In detail, murine macrophages were differentiated from bone
402 marrow cells by M-CSF stimulation and were subsequently infected with IAV, GAS or IAV and
403 GAS (Fig. 3A). We then analyzed the expression patterns of immunologically relevant surface
404 antigens by flow cytometry. In order to gain insight into differentially expressed macrophage
405 markers, we performed dimension reductions on our multiparametric data sets by t-distributed
406 stochastic neighbor embedding (t-SNE). Fig. 3B demonstrates for the topological distribution of
407 surface marker expression levels distinct allocations of cells that were obtained from the different
408 infection models. For instance, macrophage subsets overexpressing CD80 and CD86 were
409 seemingly enriched in IAV+GAS co-infected cultures, whereas mono-infection with GAS
410 resulted in the accumulation of CD206 overexpressing macrophages. Unsupervised clustering of
411 macrophage populations on the basis of their respective expression patterns by flowSOM further
412 indicated that co-infection triggered a different response than viral or bacterial mono-infections
413 (supplementary Fig. 7).

414 In an effort to obtain a more detailed picture of IAV- and GAS-induced immune responses,
415 we next focused on the individual expressions of macrophage surface antigens. Given the inter-
416 experimental variance of macrophage cultures, median fluorescence intensities (MFI) of (co)-
417 infected cells were normalized to their corresponding uninfected controls that were acquired from
418 the same donor animal (supplementary Fig. 8). Notably, expression patterns were similar within
419 each group, which resulted in a robust hierarchical clustering for IAV, GAS and IAV+GAS
420 infected macrophages (Fig. 3C). In detail, apart from a significant upregulation of CD163
421 compared to both bacterial infection and co-infection, IAV had hardly any impact on the
422 expression of the investigated surface proteins (Fig. 3C, 3D). Conversely, GAS infection induced
423 the overexpression of TLR2, which was even amplified following co-infection (Fig. 3D). Both

424 the applications of GAS and IAV+GAS comparably prompted an elevated production of MHCII.
425 Although not statistically significant, GAS infection led to a slight downregulation of CD80,
426 which was reversed to an upregulated expression in the IAV+GAS group. Similarly, co-infection
427 triggered a minor overexpression of CD86 that was short of reaching statistical significance due
428 to a high within-group variance ($p = 0.067$, compared to uninfected). The downregulation of
429 CD163 as well as the attenuation of the GAS-induced CD206 upregulation in the IAV+GAS
430 group further supports the notion that a preceding IAV infection led to a distinct immune
431 response in macrophages during co-infection (Fig. 3D).

432 As a result of differentially affected expression landscapes, the proportions of distinctive
433 macrophage subpopulations shifted depending on the infection regimen (Fig. 3E). We found a
434 minor depletion of $CD80^{+}CD86^{+}$ cells following GAS infection ($p = 0.1$), whereas co-infection
435 caused a significantly increased proportion of this population when compared to uninfected
436 controls (Fig. 3F). Both bacterial mono-infection and co-infection induced an enrichment of
437 $MHCII^{+}$ macrophages, suggesting a retained ability of these immune cells to inform and
438 coordinate an adaptive immune response. In accordance with the altered expression profiles
439 shown in Fig. 3D, the proportions of $CD163^{+}$ and $CD206^{+}$ cells, respectively, were decreased
440 upon co-infection relative to GAS infection only (Fig. 3F).

441 Collectively, our data on the diversification of surface antigen expression demonstrated that
442 the immune response of macrophages towards co-infection with IAV and GAS was considerably
443 distinct from the effects that were induced by either mono-infection. Although we encountered
444 some similarities between the GAS and IAV+GAS groups, the preceding viral infection
445 seemingly manipulated or obliterated the macrophages´ reaction towards the bacterial pathogen.
446

447 *3.4 A preceding influenza A virus infection impaired the inflammatory capacity of*
448 *macrophages during co-infection*

449 In order to gain further insights into the immune response triggered by infected
450 macrophages, we next performed analyses on mRNA expression of immune mediators by
451 quantitative PCR and measured cytokine secretion by ELISA or bead-based multiplex analysis
452 (Fig. 4A). As illustrated in Fig. 4B, the different (co-)infection regimens triggered distinct
453 expression patterns of immunomodulatory agents that resulted in strong within-group
454 associations as shown via hierarchical clustering. IAV infection was specifically characterized by
455 a relatively higher expression of *Mgl2* and *Tgfb1* (Fig 4C, supplementary Fig. 9). Bacterial
456 infection, on the other hand, comprehensively stimulated the overexpression of several genes that
457 mediate an inflammatory response (Fig. 4B). Strikingly, co-infected macrophages mostly failed
458 to induce a similar magnitude of GAS inducible overexpression, yet upregulated *Arg1* (Fig. 4B,
459 4C).

460 By further examining individual expressions, we found that *Mgl2* was significantly reduced
461 following bacterial mono-infection and co-infection by 1.8- and 3.9-fold, respectively, compared
462 to uninfected controls (Fig. 4C). Remarkably, GAS application induced an approximately 3,000
463 fold overexpression of *Nos2* that was impeded during co-infection to a mere, yet statistically
464 significant, 10-fold overexpression. Furthermore, co-infection triggered the upregulation of *Ccl2*,
465 *Cxcl2* and *Tnf*, which were significantly less pronounced in comparison to GAS infection only
466 (Fig. 4D). Secretion of these cytokines was mostly comparable between these groups, however
467 TNFα production by co-infected macrophages was reduced (Fig. 4E). Although both *Il6* and *Il10*
468 were increased in the GAS and IAV+GAS group, respectively, only co-infection caused a
469 significant secretion of the protein products (supplementary Fig. 9). While *Ifnb1* was only
470 upregulated following GAS infection, *Tgfb1* was downregulated after GAS infection as well as

471 co-infection (supplementary Fig. 9A). Of note, although the GAS-induced overexpression of *Il1b*
472 was also observed in the IAV+GAS group, co-infection entirely abrogated the secretion of
473 mature IL-1β, which suggests that a preceding IAV infection compromised innate immune
474 sensing of Streptococci (Fig. 4D, 4E).

475 In summary, the expression patterns of immunologically active mediators were noticeably
476 different between GAS mono-infection and IAV+GAS co-infection, implying that prior virus
477 infection modifies anti-streptococcal immunity.

478

479 # 4 Discussion

480 In this study we demonstrated that influenza promoted subsequent GAS-induced
481 bacteremia and allowed for an unopposed dissemination of the bacterial pathogen within the
482 blood and its migration into lungs as well as synovial tissues. Although we did not assess any
483 alterations in bone or cartilage morphology, we would like to argue that an invasion of articular
484 tissue by GAS is reminiscent of septic arthritis [37]. Indeed, we previously demonstrated that the
485 occurrence of paw edemas, which in the present study was more likely during IAV and GAS co-
486 infection, was due to bacterial colonization of both, subcutaneous and periarticular tissues and
487 was paralleled by immune cell infiltration [32]. Hence, we here show for the first time, that a
488 preceding IAV infection predisposes the host to severe complications during GAS blood
489 infection. Conversely, IAV infection elicited subsequent to GAS bacteremia did not aggravate
490 disease severity, suggesting that immune priming events in response to a prior viral encounter
491 incapacitate an otherwise competent anti-bacterial immune response.

492 Influenza in humans is usually characterized by mild-to-moderate disease that is rarely
493 lethal and resolves shortly after infection [38], which was also shown in our animal model of IAV
494 inoculation. Upon entry into nasopharyngeal cavities, the virus trespasses into the mucus, invades
495 the epithelium and spreads to immune cells [39,40]. The host then recognizes parts of the viral
496 RNA genome by intracellular pattern recognitions receptors, which triggers the production of
497 several inflammatory cytokines, among them type I IFNs, that establish an anti-viral immune
498 state [41–43]. We have demonstrated that residual viral genes persisted for 16 days in the lungs
499 of some infected mice, which was paralleled by a continuous upregulation of *Ifnb1*. However, we
500 believe it to be unlikely that replicative viral particles were still present in the lungs up to this
501 point because IAV is typically cleared within a couple days following infection [44–46]. Type I
502 IFN can have beneficial effects during bacterial infection by promoting host resilience and by

503 preventing systemic hyperinflammation [47–50]. However, several studies advocated that the
504 consequences of type I IFN expression are detrimental for the containment of a secondary
505 bacterial insult subsequent to influenza [20,51,52].

506 By using a mouse strain that lacks the common IFNα/β receptor (IFNAR) in a model of
507 pneumococcal superinfection, Shahangian and colleagues demonstrated that the IAV-induced
508 IFNAR signaling led to an impaired production of the neutrophil attractants CXCL1 and CXCL2
509 [22]. They argued that, in agreement with a complementary study by Didierlaurent *et al*., type I
510 IFNs desensitize subsequent TLR-mediated recognition of bacterial components by macrophages,
511 which are major producers for these chemokines [22,23]. Another work on IFNAR$^{-/-}$ mice by
512 Nakamura and colleagues had some contrasting results concerning the impact of type I IFN
513 signaling on pneumococcal superinfection [24]. In their study, they found that the virus and the
514 bacteria were capable of synergistically inducing an overproduction of type I IFNs, which led to
515 an impaired production of CCL2 while CXCL1/2 production was unaltered [24,53]. CCL2
516 supports bacterial clearance by the attraction of CCR2^{+} monocytes to the infected tissue [54,55].
517 Along these lines, we found in our study that CCL2 was significantly reduced in the plasma of
518 IAV-infected mice and that both, monocausal bacterial infection and co-infection featured *Ifnb1*
519 overexpression in the lung. Hence, although the role of CCL2 during GAS infections is not yet
520 fully elucidated, we propose a mode in which a preceding influenza restricts anti-bacterial
521 immunity by limiting monocyte homing and their differentiation to macrophages not only in
522 pulmonary tissues but also in remote host compartments that would be affected during
523 bacteremia.

524 Apart from the ramifications due to an impaired chemokinogenesis, we suspected other
525 means by which IAV dampens innate immune sensing of GAS. We hence focused on
526 macrophage immunobiology in the context of co-infection and found that the virus

527 comprehensively altered GAS-induced gene expression patterns and cytokine layout. In detail,
528 we detected that the immune sensors CD163 and CD206 were markedly downregulated in co-
529 infected compared to GAS only infected macrophages. CD163 is an acute phase-regulated
530 scavenger receptor that is exclusively expressed by cells of the monocyte lineage and aids in the
531 removal of potentially toxic iron complexes during intravascular hemolysis [56–59]. Due to the
532 fact that CD163 also mediates tissue repair [60], host resilience [56,58], immune resolution and is
533 able to sense gram-positive bacteria [61,62], we speculate that this receptor might confer a
534 protective immune state during hemolytic bacteremia, even though its role in GAS infection is
535 yet underexplored. Similarly, the mannose receptor CD206 might support pathogen sensing
536 during co-infection [63–67], however mice that lack this sensor molecule are not more
537 susceptible to bacterial infection [68,69].

538 Strikingly, a preceding IAV inoculation notably reduced the GAS-induced upregulation of
539 *Nos2* while boosting *Arg1* expression. Both genes code for enzymes that compete for the
540 substrate L-Arginine, yet induce opposed immune mechanisms [70–72]. While nitric oxide
541 synthase 2 (NOS2) provides inflammatory and bactericidal metabolites [73–75], arginase
542 (ARG1) supports tissue repair and immune resolution [73]. Thus, our data hint at a distortion of
543 anti-bacterial processes due to a prior IAV infection. This is further corroborated by an
544 inadequate sensing of the bacterial pathogen indicated by the reduced and abolished production
545 of TNFα and IL-1β, respectively, which was similarly shown in a model of pneumococcal
546 superinfection [19]. Interestingly, we detected for both, GAS mono-infection and superinfection
547 an upregulation of *Il1b*, which suggests that the incapacity of co-infected macrophages to process
548 and secrete IL-1β is due to a failure in the GAS-inducible activation of the NLRP3
549 inflammasome [76–79]. In fact, it was shown that different variants of IAV, including a 2009
550 pandemic strain, were capable of thwarting IL-1β maturation by interfering with NLRP3

551 inflammasome assembly [80–82], which is crucial for innate immune sensing and coordination
552 [83]. An IAV-mediated nullification of IL-1β secretion would be of dramatic consequences
553 during streptococcal superinfection. The absence of signaling via the IL-1 receptor (IL-1R) was
554 in fact associated with an increased susceptibility to systemic GAS infection in both mice and
555 humans [76,84,85]. Remarkably, rheumatoid arthritis patients that received the IL-1R antagonist
556 Anakinra exhibited a roughly 330-fold increased rate of invasive GAS infections which included
557 an elevated likelihood of life-threatening complications such as necrotizing fasciitis and sepsis
558 [85].

559 In summary, we here describe in complementary *in vivo* and *in vitro* co-infection model
560 that IAV infection paralyses anti-streptococcal innate immunity. This finding warrants further
561 investigations on the mechanisms underlying this phenomenon that sets the stage for post-
562 influenza superinfection. As an important side issue, our work underscores the importance of
563 regular vaccinations against influenza in order to avert bacterial superinfection and prevent fatal
564 invasive GAS complications [10,86–90].

565 # References

566 1. Siemens N, Oehmcke-Hecht S, Mettenleiter TC, Kreikemeyer B, Valentin-Weigand P, Hammerschmidt S.
567 Port d'Entrée for Respiratory Infections – Does the Influenza A Virus Pave the Way for Bacteria? Front
568 Microbiol. 2017;8: 2602. doi:10.3389/fmicb.2017.02602

569 2. Tjon-Kon-Fat R, Meerhoff T, Nikisins S, Pires J, Pereyaslov D, Gross D, et al. The potential risks and
570 impact of the start of the 2015–2016 influenza season in the WHO European Region: a rapid risk assessment.
571 Influenza Other Respi Viruses. 2016;10: 236–246. doi:10.1111/irv.12381

572 3. McHardy AC, Adams B. The Role of Genomics in Tracking the Evolution of Influenza A Virus. Manchester
573 M, editor. PLoS Pathog. 2009;5: e1000566. doi:10.1371/journal.ppat.1000566

574 4. Neumann G, Noda T, Kawaoka Y. Emergence and pandemic potential of swine-origin H1N1 influenza virus.
575 Nature. 2009;459: 931–939. doi:10.1038/nature08157

576 5. Taubenberger JK, Morens DM. 1918 Influenza: the mother of all pandemics. Emerg Infect Dis. 2006;12: 15–
577 22. doi:10.3201/eid1201.050979

578 6. Morens DM, Taubenberger JK, Fauci AS. Predominant Role of Bacterial Pneumonia as a Cause of Death in
579 Pandemic Influenza: Implications for Pandemic Influenza Preparedness. J Infect Dis. 2008;198: 962–970.
580 doi:10.1086/591708

581 7. Brundage JF, Shanks GD. Deaths from Bacterial Pneumonia during 1918–19 Influenza Pandemic. Emerg
582 Infect Dis. 2008;14: 1193–1199. doi:10.3201/eid1408.071313

583 8. Tasher D, Stein M, Simões EAF, Shohat T, Bromberg M, Somekh E. Invasive bacterial infections in relation
584 to influenza outbreaks, 2006-2010. Clin Infect Dis. 2011;53: 1199–1207. doi:10.1093/cid/cir726

585 9. McKenna S, Malito E, Rouse SL, Abate F, Bensi G, Chiarot E, et al. Structure, dynamics and
586 immunogenicity of a catalytically inactive CXC chemokine-degrading protease SpyCEP from Streptococcus
587 pyogenes. Comput Struct Biotechnol J. 2020;18: 650–660. doi:10.1016/j.csbj.2020.03.004

588 10. Chaussee MS, Sandbulte HR, Schuneman MJ, DePaula FP, Addengast LA, Schlenker EH, et al. Inactivated
589 and live, attenuated influenza vaccines protect mice against influenza:Streptococcus pyogenes super-
590 infections. Vaccine. 2011;29: 3773–3781. doi:10.1016/j.vaccine.2011.03.031

591 11. Teymournejad O, Montgomery CP. Evasion of Immunological Memory by S. aureus Infection: Implications
592 for Vaccine Design. Front Immunol. 2021;12. doi:10.3389/fimmu.2021.633672

593 12. Okamoto S, Kawabata S, Nakagawa I, Okuno Y, Goto T, Sano K, et al. Influenza A Virus-Infected Hosts
594 Boost an Invasive Type of Streptococcus pyogenes Infection in Mice. J Virol. 2003;77: 4104–4112.
595 doi:10.1128/JVI.77.7.4104-4112.2003
596 13. Okamoto S, Kawabata S, Terao Y, Fujitaka H, Okuno Y, Hamada S. The Streptococcus pyogenes capsule is
597 required for adhesion of bacteria to virus-infected alveolar epithelial cells and lethal bacterial-viral
598 superinfection. Infect Immun. 2004;72: 6068–6075. doi:10.1128/IAI.72.10.6068-6075.2004
599 14. van der Sluijs KF, Nijhuis M, Levels JHM, Florquin S, Mellor AL, Jansen HM, et al. Influenza-induced
600 expression of indoleamine 2,3-dioxygenase enhances interleukin-10 production and bacterial outgrowth
601 during secondary pneumococcal pneumonia. J Infect Dis. 2006;193: 214–22. doi:10.1086/498911
602 15. Wang B, Li S, Southern PJ, Cleary PP. Streptococcal modulation of cellular invasion via TGF-β1 signaling.
603 Proc Natl Acad Sci. 2006;103: 2380–2385. doi:10.1073/pnas.0506668103
604 16. Herrera AL, Suso K, Allison S, Simon A, Schlenker E, Huber VC, et al. Binding host proteins to the M
605 protein contributes to the mortality associated with influenza–streptococcus pyogenes superinfections.
606 Microbiol (United Kingdom). 2017;163: 1445–1456. doi:10.1099/mic.0.000532
607 17. Korteweg C, Gu J. Pathology, Molecular Biology, and Pathogenesis of Avian Influenza A (H5N1) Infection
608 in Humans. Am J Pathol. 2008;172: 1155–1170. doi:10.2353/ajpath.2008.070791
609 18. Plotkowski MC, Bajolet-Laudinat O, Puchelle E. Cellular and molecular mechanisms of bacterial adhesion to
610 respiratory mucosa. Eur Respir J. 1993;6: 903–16. Available: http://www.ncbi.nlm.nih.gov/pubmed/8339812
611 19. Sun K, Metzger DW. Inhibition of pulmonary antibacterial defense by interferon-γ during recovery from
612 influenza infection. Nat Med. 2008;14: 558–564. doi:10.1038/nm1765
613 20. Navarini AA, Recher M, Lang KS, Georgiev P, Meury S, Bergthaler A, et al. Increased susceptibility to
614 bacterial superinfection as a consequence of innate antiviral responses. Proc Natl Acad Sci. 2006;103:
615 15535–15539. doi:10.1073/pnas.0607325103
616 21. Metzger DW, Sun K. Immune Dysfunction and Bacterial Coinfections following Influenza. J Immunol.
617 2013;191: 2047–2052. doi:10.4049/jimmunol.1301152
618 22. Shahangian A, Chow EK, Tian X, Kang JR, Ghaffari A, Liu SY, et al. Type I IFNs mediate development of
619 postinfluenza bacterial pneumonia in mice. J Clin Invest. 2009;119: 1910–1920. doi:10.1172/JCI35412
620 23. Didierlaurent A, Goulding J, Patel S, Snelgrove R, Low L, Bebien M, et al. Sustained desensitization to
621 bacterial Toll-like receptor ligands after resolution of respiratory influenza infection. J Exp Med. 2008;205:

622 323–329. doi:10.1084/jem.20070891
623 24. Nakamura S, Davis KM, Weiser JN. Synergistic stimulation of type I interferons during influenza virus
624 coinfection promotes Streptococcus pneumoniae colonization in mice. J Clin Invest. 2011;121: 3657–3665.
625 doi:10.1172/JCI57762
626 25. Cunningham MW. Pathogenesis of Group A Streptococcal Infections. Clin Microbiol Rev. 2000;13: 470–
627 511. doi:10.1128/CMR.13.3.470-511.2000
628 26. Musher D. Trends in Bacteremic Infection Due to Streptococcus pyogenes (Group A Streptococcus), 1986-
629 1995. Emerg Infect Dis. 1996;2: 54–56. doi:10.3201/eid0201.960107
630 27. Herrera AL, Huber VC, Chaussee MS. The association between invasive group A streptococcal diseases and
631 viral respiratory tract infections. Front Microbiol. 2016;7: 1–7. doi:10.3389/fmicb.2016.00342
632 28. Goldmann O, Rohde M, Chhatwal GS, Medina E. Role of Macrophages in Host Resistance to Group A
633 Streptococci. Infect Immun. 2004;72: 2956–2963. doi:10.1128/IAI.72.5.2956-2963.2004
634 29. Ghoneim HE, Thomas PG, McCullers JA. Depletion of Alveolar Macrophages during Influenza Infection
635 Facilitates Bacterial Superinfections. J Immunol. 2013;191: 1250–1259. doi:10.4049/jimmunol.1300014
636 30. Schultz D, Methling K, Rothe M, Lalk M. Eicosanoid Profile of Influenza A Virus Infected Pigs.
637 Metabolites. 2019;9: 130. doi:10.3390/metabo9070130
638 31. Miller MA, Stabenow JM, Parvathareddy J, Wodowski AJ, Fabrizio TP, Bina XR, et al. Visualization of
639 Murine Intranasal Dosing Efficiency Using Luminescent Francisella tularensis: Effect of Instillation Volume
640 and Form of Anesthesia. Kaushal D, editor. PLoS One. 2012;7: e31359. doi:10.1371/journal.pone.0031359
641 32. Volzke J, Schultz D, Kordt M, Müller M, Bergmann W, Methling K, et al. Inflammatory Joint Disease Is a
642 Risk Factor for Streptococcal Sepsis and Septic Arthritis in Mice. Front Immunol. 2020;11: 1–15.
643 doi:10.3389/fimmu.2020.579475
644 33. Shrum B, Anantha R V., Xu SX, Donnelly M, Haeryfar S, McCormick JK, et al. A robust scoring system to
645 evaluate sepsis severity in an animal model. BMC Res Notes. 2014;7: 233. doi:10.1186/1756-0500-7-233
646 34. Amend SR, Valkenburg KC, Pienta KJ. Murine Hind Limb Long Bone Dissection and Bone Marrow
647 Isolation. J Vis Exp. 2016;110. doi:10.3791/53936
648 35. Belkina AC, Ciccolella CO, Anno R, Halpert R, Spidlen J, Snyder-Cappione JE. Automated optimized
649 parameters for T-distributed stochastic neighbor embedding improve visualization and analysis of large
650 datasets. Nat Commun. 2019;10: 1–26. doi:10.1038/s41467-019-13055-y

651 36. Van Gassen S, Callebaut B, Van Helden MJ, Lambrecht BN, Demeester P, Dhaene T, et al. FlowSOM:
652 Using self-organizing maps for visualization and interpretation of cytometry data. Cytom Part A. 2015;87:
653 636–645. doi:10.1002/cyto.a.22625
654 37. Newman JH. Review of septic arthritis throughout the antibiotic era. Ann Rheum Dis. 1976;35: 198–205.
655 doi:10.1136/ard.35.3.198
656 38. Layne SP, Beugelsdijk TJ, Patel CKN, Taubenberger JK, Cox NJ, Gust ID, et al. A Global Lab Against
657 Influenza. Science. 2001;293: 1729–1729. doi:10.1126/science.293.5536.1729
658 39. Manicassamy B, Manicassamy S, Belicha-Villanueva A, Pisanelli G, Pulendran B, Garcia-Sastre A. Analysis
659 of in vivo dynamics of influenza virus infection in mice using a GFP reporter virus. Proc Natl Acad Sci.
660 2010;107: 11531–11536. doi:10.1073/pnas.0914994107
661 40. Perrone LA, Plowden JK, García-Sastre A, Katz JM, Tumpey TM. H5N1 and 1918 Pandemic Influenza
662 Virus Infection Results in Early and Excessive Infiltration of Macrophages and Neutrophils in the Lungs of
663 Mice. Baric RS, editor. PLoS Pathog. 2008;4: e1000115. doi:10.1371/journal.ppat.1000115
664 41. Iwasaki A, Pillai PS. Innate immunity to influenza virus infection. Nat Rev Immunol. 2014;14: 315–328.
665 doi:10.1038/nri3665
666 42. Tough DF, Borrow P, Sprent J. Induction of Bystander T Cell Proliferation by Viruses and Type I Interferon
667 in Vivo. Science. 1996;272: 1947–1950. doi:10.1126/science.272.5270.1947
668 43. Matikainen S, Pirhonen J, Miettinen M, Lehtonen A, Govenius-Vintola C, Sareneva T, et al. Influenza A and
669 Sendai Viruses Induce Differential Chemokine Gene Expression and Transcription Factor Activation in
670 Human Macrophages. Virology. 2000;276: 138–147. doi:10.1006/viro.2000.0542
671 44. Ip DKM, Lau LLH, Leung NHL, Fang VJ, Chan K-H, Chu DKW, et al. Viral shedding and transmission
672 potential of asymptomatic and pauci-symptomatic influenza virus infections in the community. Clin Infect
673 Dis. 2016; ciw841. doi:10.1093/cid/ciw841
674 45. Schwaiger T, Sehl J, Karte C, Schäfer A, Hühr J, Mettenleiter TC, et al. Experimental H1N1pdm09 infection
675 in pigs mimics human seasonal influenza infections. PLoS One. 2019;14: 1–21.
676 doi:10.1371/journal.pone.0222943
677 46. Cuypers F, Schäfer A, Skorka SB, Surabhi S, Tölken LA, Paulikat AD, et al. Innate immune responses at the
678 asymptomatic stage of influenza A viral infections of Streptococcus pneumoniae colonized and non-
679 colonized mice. Sci Rep. 2021;11: 1–14. doi:10.1038/s41598-021-00211-y

680 47. Kovarik P, Castiglia V, Ivin M, Ebner F. Type I interferons in bacterial infections: A balancing act. Front
681 Immunol. 2016;7: 1–8. doi:10.3389/fimmu.2016.00652
682 48. Castiglia V, Piersigilli A, Ebner F, Janos M, Goldmann O, Damböck U, et al. Type I Interferon Signaling
683 Prevents IL-1β-Driven Lethal Systemic Hyperinflammation during Invasive Bacterial Infection of Soft
684 Tissue. Cell Host Microbe. 2016;19: 375–387. doi:10.1016/j.chom.2016.02.003
685 49. LeMessurier KS, Häcker H, Chi L, Tuomanen E, Redecke V. Type I Interferon Protects against
686 Pneumococcal Invasive Disease by Inhibiting Bacterial Transmigration across the Lung. Sullam PM, editor.
687 PLoS Pathog. 2013;9: e1003727. doi:10.1371/journal.ppat.1003727
688 50. Maier BB, Hladik A, Lakovits K, Korosec A, Martins R, Kral JB, et al. Type I interferon promotes alveolar
689 epithelial type II cell survival during pulmonary Streptococcus pneumoniae infection and sterile lung injury
690 in mice. Eur J Immunol. 2016;46: 2175–2186. doi:10.1002/eji.201546201
691 51. Antonelli LRV, Gigliotti Rothfuchs A, Gonçalves R, Roffê E, Cheever AW, Bafica A, et al. Intranasal Poly-
692 IC treatment exacerbates tuberculosis in mice through the pulmonary recruitment of a pathogen-permissive
693 monocyte/macrophage population. J Clin Invest. 2010;120: 1674–1682. doi:10.1172/JCI40817
694 52. Jia T, Leiner I, Dorothee G, Brandl K, Pamer EG. MyD88 and Type I Interferon Receptor-Mediated
695 Chemokine Induction and Monocyte Recruitment during Listeria monocytogenes Infection. J Immunol.
696 2009;183: 1271–1278. doi:10.4049/jimmunol.0900460
697 53. Zimmerer JM, Lesinski GB, Radmacher MD, Ruppert A, Carson WE. STAT1-dependent and STAT1-
698 independent gene expression in murine immune cells following stimulation with interferon-alpha. Cancer
699 Immunol Immunother. 2007;56: 1845–1852. doi:10.1007/s00262-007-0329-9
700 54. Zhang Z, Clarke TB, Weiser JN. Cellular effectors mediating Th17-dependent clearance of pneumococcal
701 colonization in mice. J Clin Invest. 2009. doi:10.1172/JCI36731
702 55. Davis KM, Nakamura S, Weiser JN. Nod2 sensing of lysozyme-digested peptidoglycan promotes
703 macrophage recruitment and clearance of S. pneumoniae colonization in mice. J Clin Invest. 2011;121:
704 3666–3676. doi:10.1172/JCI57761
705 56. Kristiansen M, Graversen JH, Jacobsen C, Sonne O, Hoffman H-J, Law SKA, et al. Identification of the
706 haemoglobin scavenger receptor. Nature. 2001;409: 198–201. doi:10.1038/35051594
707 57. Pulford K, Micklem K, McCarthy S, Cordell J, Jones M, Mason DY. A monocyte/macrophage antigen
708 recognized by the four antibodies GHI/61, Ber-MAC3, Ki-M8 and SM4. Immunology. 1992;75: 588–95.

709 Available: http://www.ncbi.nlm.nih.gov/pubmed/1592433
710 58. Buechler C, Ritter M, Orsó E, Langmann T, Klucken J, Schmitz G. Regulation of scavenger receptor CD163
711 expression in human monocytes and macrophages by pro- and antiinflammatory stimuli. J Leukoc Biol.
712 2000;67: 97–103. Available: http://www.ncbi.nlm.nih.gov/pubmed/10648003
713 59. Oliviero S, Cortese R. The human haptoglobin gene promoter: interleukin-6-responsive elements interact
714 with a DNA-binding protein induced by interleukin-6. EMBO J. 1989;8: 1145–51. Available:
715 http://www.ncbi.nlm.nih.gov/pubmed/2787245
716 60. van den Heuvel MM, Tensen CP, van As JH, van den Berg TK, Fluitsma DM, Dijkstra CD, et al. Regulation
717 of CD163 on human macrophages: cross-linking of CD163 induces signaling and activation. J Leukoc Biol.
718 1999;66: 858–866. doi:10.1002/jlb.66.5.858
719 61. Fabriek BO, van Bruggen R, Deng DM, Ligtenberg AJM, Nazmi K, Schornagel K, et al. The macrophage
720 scavenger receptor CD163 functions as an innate immune sensor for bacteria. Blood. 2009;113: 887–892.
721 doi:10.1182/blood-2008-07-167064
722 62. Kneidl J, Löffler B, Erat MC, Kalinka J, Peters G, Roth J, et al. Soluble CD163 promotes recognition,
723 phagocytosis and killing of Staphylococcus aureus via binding of specific fibronectin peptides. Cell
724 Microbiol. 2012;14: 914–936. doi:10.1111/j.1462-5822.2012.01766.x
725 63. Reading PC, Miller JL, Anders EM. Involvement of the Mannose Receptor in Infection of Macrophages by
726 Influenza Virus. J Virol. 2000;74: 5190–5197. doi:10.1128/JVI.74.11.5190-5197.2000
727 64. Pontow SE, Kery V, Stahl PD. Mannose Receptor. Int Rev Cytol. 1993;137: 221–244. doi:10.1016/S0074-
728 7696(08)62606-6
729 65. Sallusto F, Cella M, Danieli C, Lanzavecchia A. Dendritic cells use macropinocytosis and the mannose
730 receptor to concentrate macromolecules in the major histocompatibility complex class II compartment:
731 downregulation by cytokines and bacterial products. J Exp Med. 1995;182: 389–400.
732 doi:10.1084/jem.182.2.389
733 66. Stahl PD. The Macrophage Mannose Receptor: Current Status. Am J Respir Cell Mol Biol. 1990;2: 317–318.
734 doi:10.1165/ajrcmb/2.4.317
735 67. Upham JP, Pickett D, Irimura T, Anders EM, Reading PC. Macrophage Receptors for Influenza A Virus:
736 Role of the Macrophage Galactose-Type Lectin and Mannose Receptor in Viral Entry. J Virol. 2010;84:
737 3730–3737. doi:10.1128/JVI.02148-09

738 68. Lee SJ, Zheng N-Y, Clavijo M, Nussenzweig MC. Normal Host Defense during Systemic Candidiasis in
739 Mannose Receptor-Deficient Mice. Infect Immun. 2003;71: 437–445. doi:10.1128/IAI.71.1.437-445.2003
740 69. Swain SD, Lee SJ, Nussenzweig MC, Harmsen AG. Absence of the Macrophage Mannose Receptor in Mice
741 Does Not Increase Susceptibility to Pneumocystis carinii Infection In Vivo. Infect Immun. 2003;71: 6213–
742 6221. doi:10.1128/IAI.71.11.6213-6221.2003
743 70. Gordon S. Alternative activation of macrophages. Nat Rev Immunol. 2003;3: 23–35. doi:10.1038/nri978
744 71. Wu G, Morris SM. Arginine metabolism: nitric oxide and beyond. Biochem J. 1998;336: 1–17.
745 doi:10.1042/bj3360001
746 72. Starikova EA, Sokolov A V., Burova LA, Golovin AS, Lebedeva AM, Vasilyev VB, et al. The Role of
747 Arginine Deaminase from Streptococcus pyogenes in Inhibition Macrophages Nitrogen Monooxide (NO)
748 Synthesis. Russ J Infect Immun. 2018;8: 211–218. doi:10.15789/2220-7619-2018-2-211-218
749 73. Hesse M, Modolell M, La Flamme AC, Schito M, Fuentes JM, Cheever AW, et al. Differential Regulation of
750 Nitric Oxide Synthase-2 and Arginase-1 by Type 1/Type 2 Cytokines In Vivo: Granulomatous Pathology Is
751 Shaped by the Pattern of l-Arginine Metabolism. J Immunol. 2001;167: 6533–6544.
752 doi:10.4049/jimmunol.167.11.6533
753 74. Serbina N V, Salazar-Mather TP, Biron CA, Kuziel WA, Pamer EG. TNF/iNOS-Producing Dendritic Cells
754 Mediate Innate Immune Defense against Bacterial Infection. Immunity. 2003;19: 59–70. doi:10.1016/S1074-
755 7613(03)00171-7
756 75. Tavares LP, Teixeira MM, Garcia CC. The inflammatory response triggered by Influenza virus: a two edged
757 sword. Inflamm Res. 2017;66: 283–302. doi:10.1007/s00011-016-0996-0
758 76. Richter J, Brouwer S, Schroder K, Walker MJ. Inflammasome activation and IL-1β signalling in group A
759 Streptococcus disease. Cell Microbiol. 2021;23: 1–9. doi:10.1111/cmi.13373
760 77. Harder J, Franchi L, Munoz-Planillo R, Park J-H, Reimer T, Nunez G. Activation of the Nlrp3
761 Inflammasome by Streptococcus pyogenes Requires Streptolysin O and NF- B Activation but Proceeds
762 Independently of TLR Signaling and P2X7 Receptor. J Immunol. 2009;183: 5823–5829.
763 doi:10.4049/jimmunol.0900444
764 78. Lin AE, Beasley FC, Keller N, Hollands A, Urbano R, Troemel ER, et al. A group a Streptococcus ADP-
765 ribosyltransferase toxin stimulates a protective interleukin 1beta-dependent macrophage immune response.
766 MBio. 2015;6: 1–12. doi:10.1128/mBio.00133-15

767 79. Valderrama JA, Riestra AM, Gao NJ, LaRock CN, Gupta N, Ali SR, et al. Group A streptococcal M protein
768 activates the NLRP3 inflammasome. Nat Microbiol. 2017;2: 1425–1434. doi:10.1038/s41564-017-0005-6
769 80. Stasakova J, Ferko B, Kittel C, Sereinig S, Romanova J, Katinger H, et al. Influenza A mutant viruses with
770 altered NS1 protein function provoke caspase-1 activation in primary human macrophages, resulting in fast
771 apoptosis and release of high levels of interleukins 1β and 18. J Gen Virol. 2005;86: 185–195.
772 doi:10.1099/vir.0.80422-0
773 81. Park HS, Lu Y, Pandey K, Liu GQ, Zhou Y. NLRP3 Inflammasome Activation Enhanced by TRIM25 is
774 Targeted by the NS1 Protein of 2009 Pandemic Influenza A Virus. Front Microbiol. 2021;12.
775 doi:10.3389/fmicb.2021.778950
776 82. Pothlichet J, Meunier I, Davis BK, Ting JP-Y, Skamene E, von Messling V, et al. Type I IFN Triggers RIG-
777 I/TLR3/NLRP3-dependent Inflammasome Activation in Influenza A Virus Infected Cells. Pekosz A, editor.
778 PLoS Pathog. 2013;9: e1003256. doi:10.1371/journal.ppat.1003256
779 83. Lamotte LA, Tafforeau L. How influenza a virus ns1 deals with the ubiquitin system to evade innate
780 immunity. Viruses. 2021;13: 1–26. doi:10.3390/v13112309
781 84. Midiri A, Mancuso G, Beninati C, Gerace E, Biondo C. The relevance of il-1-signaling in the protection
782 against gram-positive bacteria. Pathogens. 2021;10: 1–13. doi:10.3390/pathogens10020132
783 85. LaRock CN, Todd J, LaRock DL, Olson J, O'Donoghue AJ, Robertson AAB, et al. IL-1β is an innate
784 immune sensor of microbial proteolysis. Sci Immunol. 2016;1: eaah3539–eaah3539.
785 doi:10.1126/sciimmunol.aah3539
786 86. Ely CF. Influenza as seen at the puget sound navy yard. J Am Med Assoc. 1919;72: 24.
787 doi:10.1001/jama.1919.26110010003009
788 87. Okamoto S, Kawabata S, Fujitaka H, Uehira T, Okuno Y, Hamada S. Vaccination with formalin-inactivated
789 influenza vaccine protects mice against lethal influenza Streptococcus pyogenes superinfection. Vaccine.
790 2004;22: 2887–2893. doi:10.1016/j.vaccine.2003.12.024
791 88. Grabenstein JD. Immunization to Protect the US Armed Forces: Heritage, Current Practice, and Prospects.
792 Epidemiol Rev. 2006;28: 3–26. doi:10.1093/epirev/mxj003
793 89. Ozgur SK, Beyazova U, Kemaloglu YK, Maral I, Sahin F, Camurdan AD, et al. Effectiveness of Inactivated
794 Influenza Vaccine for Prevention of Otitis Media in Children. Pediatr Infect Dis J. 2006;25: 401–404.
795 doi:10.1097/01.inf.0000217370.83948.51

90. Clements DA. Influenza A Vaccine Decreases the Incidence of Otitis Media in 6- to 30-Month-Old Children in Day Care. Arch Pediatr Adolesc Med. 1995;149: 1113. doi:10.1001/archpedi.1995.02170230067009

Acknowledgment

The authors would like to thank Wendy Bergman for her excellent support during the work for this study. We also thank Dirk Koczan and Ildiko Toth for their help with the transcription analyses. Moreover, we like to express our gratitude to Karin Gerber and Chantal von Hörsten for their participation in the animal breeding and care at the animal core facility. The authors sincerely give their thanks to all staff and students that took part in the scientific discussions and experimental conduct.

Funding

This research was funded by Federal Excellence Initiative of Mecklenburg-Western Pomerania and European Social Fund (ESF) Grant KoInfekt (ESF/14-BM-A55-0011/16 and ESF/14- BM-A55-0005/16).

Ko-Infekt Study Group

Karen Methling[2], Michael Lalk[2], Ulrike Blohm[3], Alexander Schäfer[3], Bernd Kreikemeyer[4]

(Affiliations are listed on the title page)

Author Contributions

J.V. and B.M-H. designed the study. J.V., M.B., E.W., M.M., D.S., K.M., U.B. and A.S. designed and performed the experiments and collected the data. J.V., M.B. and D.S. performed the statistical analyses. J.V. wrote the first draft of the manuscript. All authors contributed to the article and approved the submitted version.

818 ## Disclosures

819 The authors have no financial conflict of interest.

820 ## Abbreviations Used in This Article

821 In order of appearance:

822 **IAV** Influenza A Virus

823 **GAS** Group A Streptococcus

824 **HA** Hemagglutinin

825 **IL** Interleukin

826 **IFN** Interferon

827 **MDCKII** Mardin-Darby Canine Kidney II (cells)

828 **TCID50** Tissue Culture Infectious Dose 50

829 **THB** Todd-Hewitt Broth

830 **CFU** Colony-forming Units

831 **20-HETE** 20-Hydroxyeicosatetraenoic acid

832 **13-HODE** 13-Hydroxyoctadecadienoic acid

833 **PGE_2** Prostanglandin E_2

834 **AA** Arachidonic Acid

835 **DMEM** Dulbecco's Modified Eagle's Medium

836 **FCS** Fetal Calf Serum

837 **M-CSF** Macrophage Colony-stimulating Factor

838 **RB** Running Buffer

839 **7-AAD** 7-Aminoactinomycin

840 **MFI** Median Fluorescence Intensity

841 **t-SNE** t-distributed stochastic neighbor embedding

842 **CCL2/MCP-1** Chemokine CC-Motif Ligand 2/Monocyte Chemoattractant Protein-1

843 **TNFα** Tumor Necrosis Factor α

844 **CXCL2/MIP2-α** Chemokine CXC-Motif Ligand 2/Macrophage Inflammatory Protein 2-α

845 **ELISA** Enzyme-linked Immunosorbent Assay

846 **ANOVA** Analysis of Variance

847 **r** Pearson Product-moment Correlation Coefficient

848 **SEM** Standard Error of the Mean

849 **IFNAR** Interferon-α/β Receptor

850 **NOS2** Nitric Oxide Synthase 2

851 **ARG1** Arginase

852 **NLRP3** NLR Family Pyrin Domain Containing 3

853 **IL-1R** Interleukin-1 Receptor

854 # Supplementary Material

855 Contents:

856 Supplementary Figure 1. Gating Strategy for the analysis of murine bone marrow derived macrophages.

857 Supplementary Figure 2. PCR Product lengths for influenza A Virus genes.

858 Supplementary Figure 3. PCR product melting curves for influenza A Virus genes.

859 Supplementary Figure 4. Eicosanoid production was not differentially regulated in paws from co-infected mice.

860 Supplementary Figure 5. PCR product lengths for Group A Streptococcus genes.

861 Supplementary Figure 6. PCR product melting curves for Group A Streptococcus genes.

862 Supplementary Figure 7. FlowSOM clutering on flow cytometry data from infected macrophages.

863 Supplementary Figure 8. Surface antigen expression changes on macrophages after infection and co-infection.

864 Supplementary Figure 9. Expression and secretion of cytokines induced by infection or co-infection.

865 Supplementary Table I. Primers for quantitative polymerase chain reaction of influenza A genes.

866 Supplementary Table II. Primers for quantitative polymerase chain reaction of Group A Streptococcus genes.

867 Supplementary Table III. Pearson correlation analyses of sepsis scores with paw eicosanoids.

868 # Figures

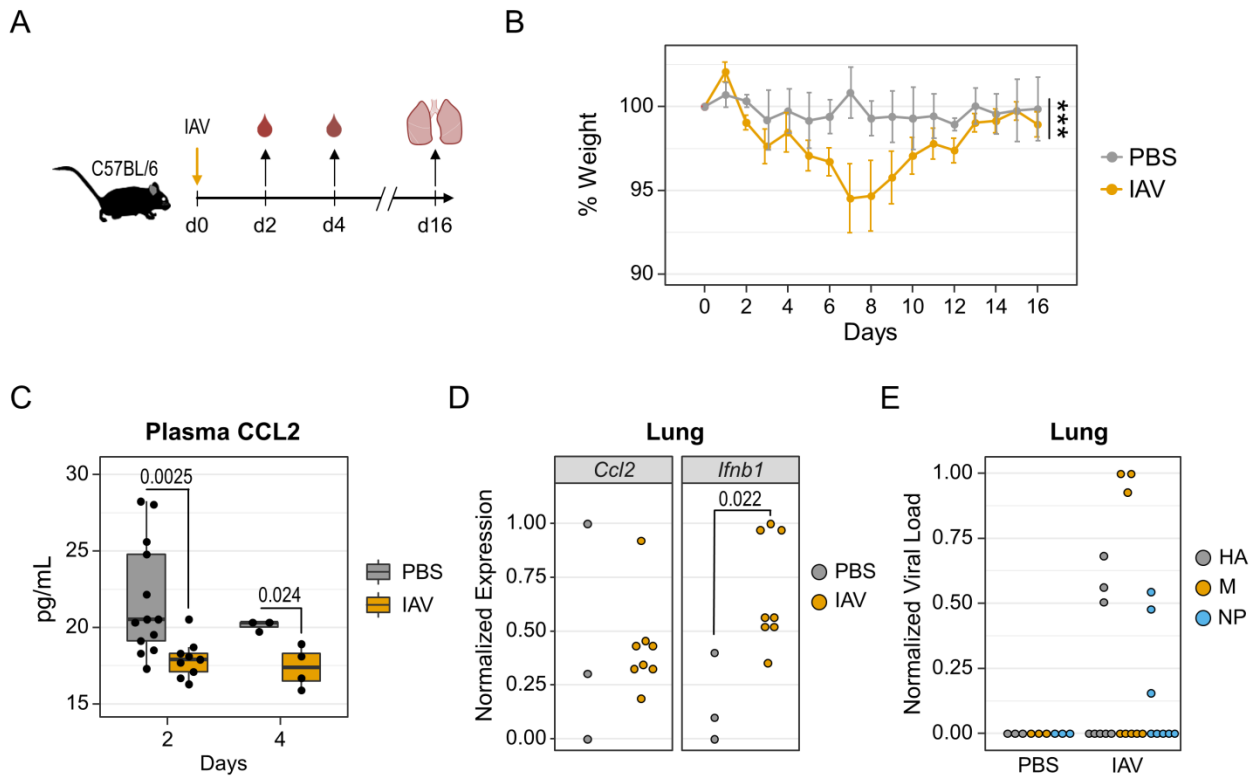

869

870 **Figure 1. Influenza A virus infection induced minor weight loss and inhibited the production of CCL2.** (**A**)
871 Experimental Design. Mice were intranasally infected with influenza A virus (IAV, n = 8, two indepentent
872 experiments). PBS was adminstered as a control (n = 3, two independent experiments). Blood samples were drawn
873 on days 2 and 4 following infection. Lungs were excised at day 16. (**B**) Mean weight changes relative to day 0.
874 Weight loss was confirmed by one-way ANOVA ($p < 0.0001$) in the IAV group and by two-way ANOVA (***$p <$
875 0.001) comparing the IAV group to PBS controls. Error bars depict the SEM. (**C**) Boxplots display CCL2
876 concentrations in plasma samples from uninfected controls (n = 13, six independent experiments) and IAV infected
877 mice (n = 9, five independent experiments). Day 2 and Day 4 p-values result from Mann-Whitney U test and t-test,
878 respectively. (**D**) Dotplots show normalized mRNA expression of *Ccl2* and *Ifnb1* in lung homogenates based on ΔCt
879 values. p-value results from t-test. (**E**) Normalized viral loads based on Ct values for IAV specific genes in day 16
880 lung homogenates.

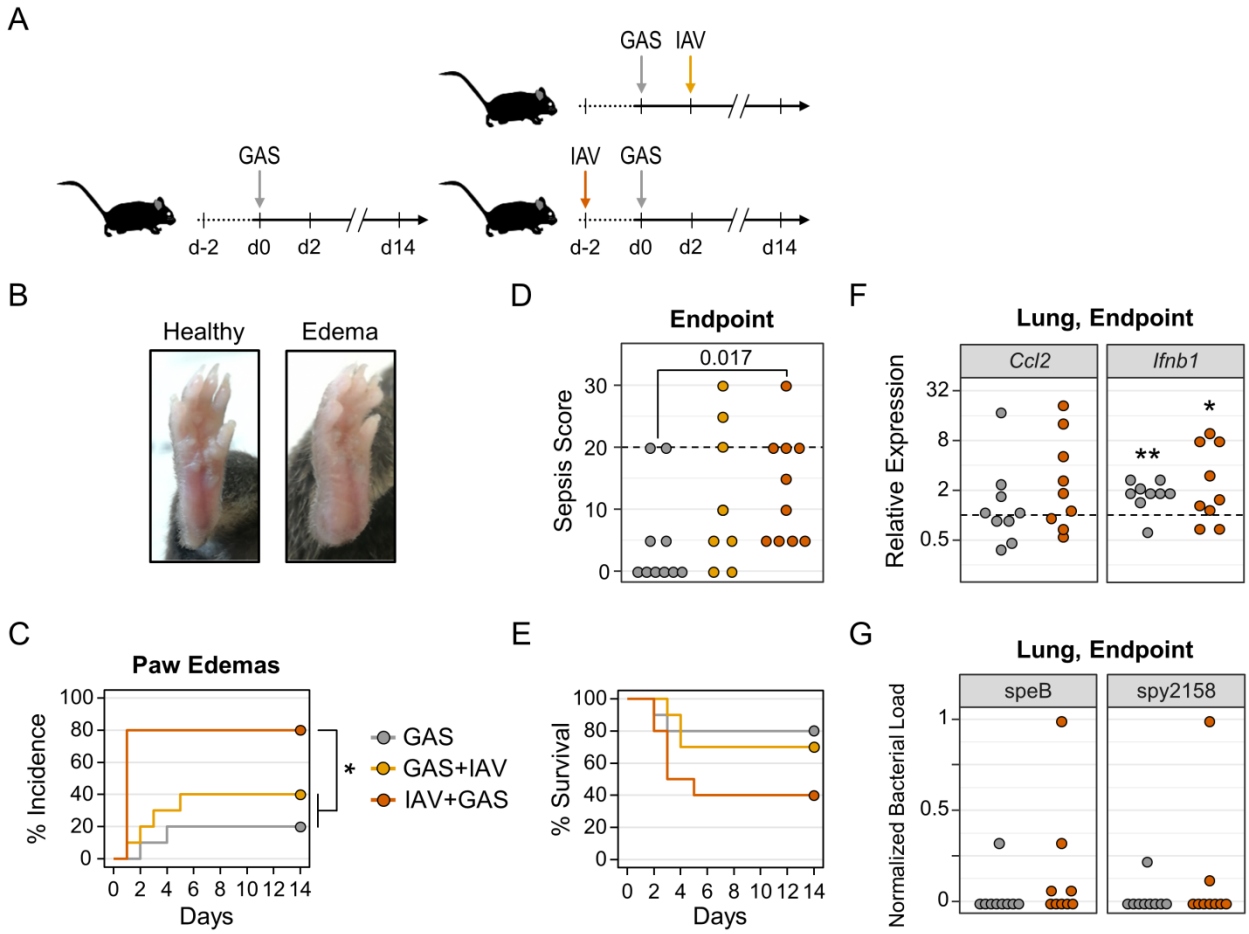

Figure 2. Preceding IAV infection promotes bacterial dissemination and sepsis severity during co-infection. (**A**) Experimental design. For monocausal bacterial infection, Group A Streptococcus was administered intravenously (GAS, n = 10, two independent experiments). For co-infection, mice were either infected with GAS followed by intranasal IAV administration (GAS+IAV, n = 10, three independent experiments) or infected with IAV followed by infection with GAS (IAV+GAS, n = 10, three independent experiments). (**B**) Representative photographies of a healthy compared to an edematous paw after IAV+GAS co-infection. (**C**) Kaplan-Meier curves display the incidences of paw edemas. *$p < 0.05$, log-rank test with p-value adjustment for multiple comparisons (Bonferroni-Holm method). (**D**) Dotplot shows sepsis scores at endpoints (day 14 or humane endpoint). p-value results from Mann-Whitney U test. The dashed line indicates the minimum score for humane endpoints. (**E**) Kaplan-Meier curves display survival probabilities. (**F**) Dotplots show endpoint bulk lung mRNA gene expressions of *Ccl2* and *Ifnb1*that were normalized to *Gapdh* and lungs from uninfected mice (dashed line) by the $2^{-\Delta\Delta Ct}$ method. *$p < 0.05$, **$p < 0.01$, one-sample Wilcoxon signed-rank test ($\mu = 1$). (**G**) Normalized bacterial loads based on Ct values for GAS specific genes in endpoint lung homogenates.

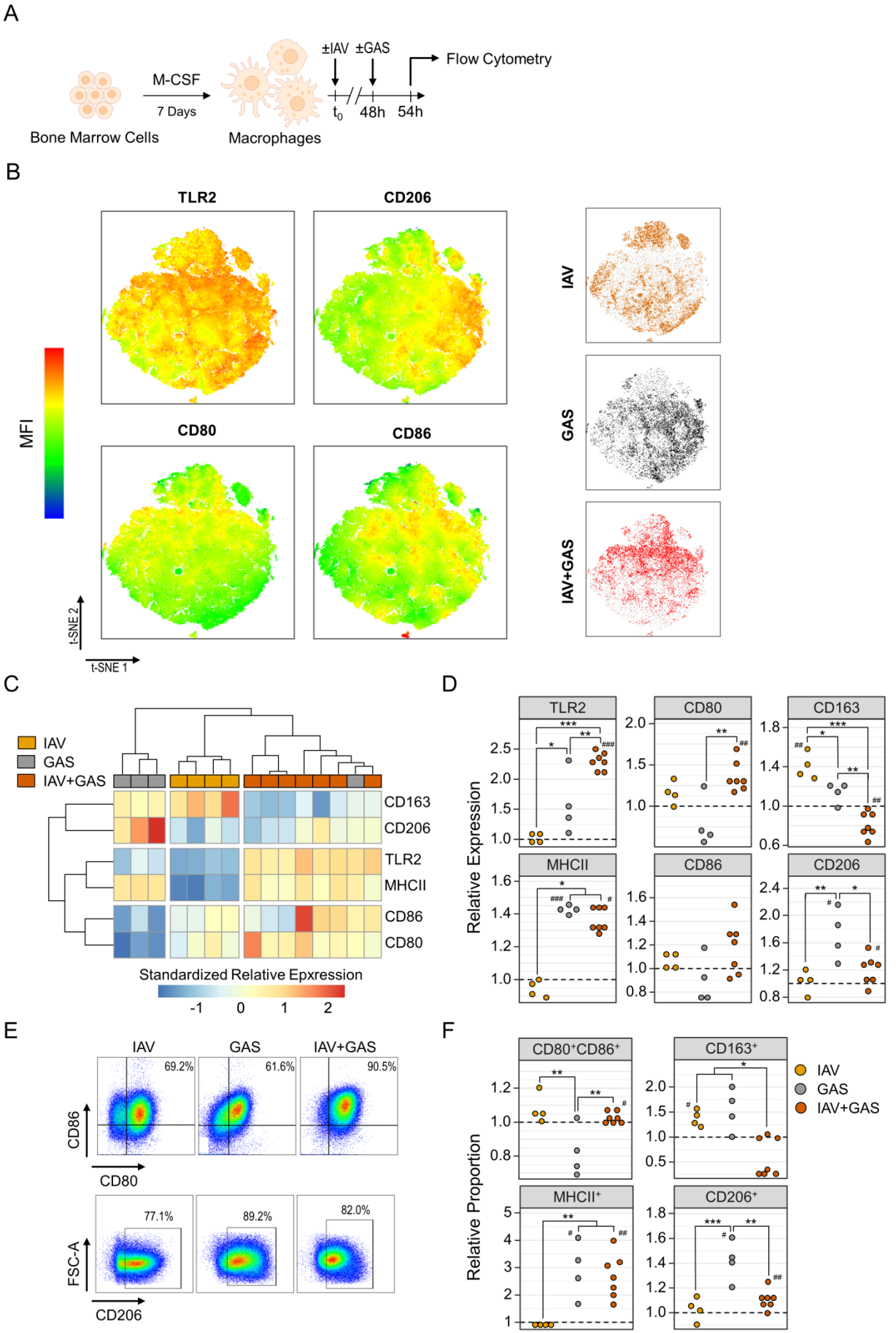
A
M-CSF
7 Days
Bone Marrow Cells
Macrophages
±IAV ±GAS
Flow Cytometry
t0
48h
54h
B
TLR2
CD206
CD80
CD86
MFI
t-SNE 2
t-SNE 1
IAV
GAS
IAV+GAS
C
IAV
GAS
IAV+GAS
CD163
CD206
TLR2
MHCII
CD86
CD80
Standardized Relative Epxression
-1
0
1
2
D
TLR2
CD80
CD163
MHCII
CD86
CD206
Relative Expression
E
IAV
GAS
IAV+GAS
69.2%
61.6%
90.5%
CD86
CD80
77.1%
89.2%
82.0%
FSC-A
CD206
F
CD80+CD86+
CD163+
MHCII+
CD206+
Relative Proportion
IAV
GAS
IAV+GAS

895

896 **Figure 3. Activation of bone-marrow derived murine macrophages during *in vitro* co-infection was distinct**
897 **from bacterial mono-infection.** (**A**) Experimental Design. Macrophages were differentiated from bone marrow cells
898 and then infected with either IAV for 48 h (n = 4) or GAS for 6 h (n = 4). For co-infection, IAV was first applied for
899 48 h followed by GAS infection for 6 h (IAV+GAS, n = 7). Each sample was obtained from individual mice to
900 obtain biological replicates. All data were generated as four independent experiments. (**B**) t-distributed stochastic
901 neighbor embedding (tSNE) on flow cytometry data from infected macrophages and topology of surface antigen
902 expression levels. 10,000 events from each sample were integrated into the dimension reduction analysis. MFI:
903 median fluorescence intensity. (**C**) Heatmap and hierarchical clustering on standardized fold changes of surface
904 antigen expression levels based on their MFI. Fold changes were generated by normalization of MFI data from
905 infected macrophages to their respective paired uninfected controls. (**D**) Dotplots depict the alteration of surface
906 antigen expression levels due to (co-)infection. (**E**) Representative pseudocolor plots illustrate the alteration of
907 proportions of macrophages expressing CD80 and CD86 (top) or CD206 (bottom) after (co-)infection. (**F**) Dotplots
908 demonstrate the shift of macrophage subpopulation fractions after (co-)infection relative to uninfected controls
909 (dashed lines). $^{*}p < 0.05$, $^{**}p < 0.01$, $^{***}p < 0.001$, Dunn's test or Tukey HSD test with p-value adjustments for
910 multiple comparisons (Bonferroni-Holm method). $^{\#}p < 0.05$, $^{\#\#}p < 0.01$, $^{\#\#\#}p < 0.001$, Wilcoxon signed-rank test or
911 one-sample t-test for the comparison to uninfected cultures ($\mu = 1$).

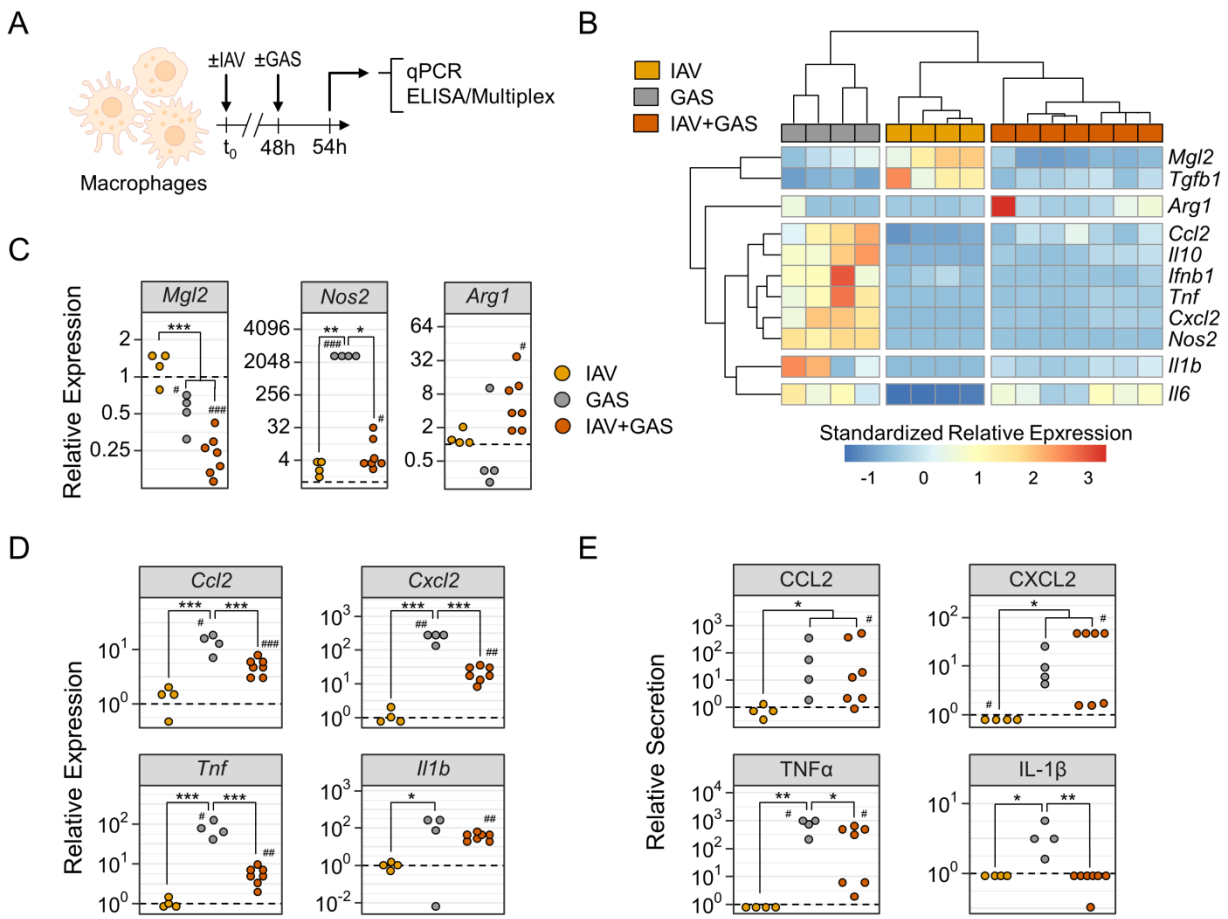

Figure 4. Preceeding influenza A virus infection impedes pro-inflammatory immunological features of macrophages during co-infection. (**A**) Experimental Design. Bone-marrow derived macrophages were infected with IAV (n = 4), GAS (n = 4) or IAV+GAS (n = 7). Each sample was obtained from individual mice to obtain biological replicates. All data were generated as four independent experiments. (**B**) Heatmap and hierarchical clustering on standardized relative mRNA expression levels from quantitative PCR analyses using the $2^{-\Delta\Delta Ct}$ method. Data from infected cultures were normalized to *Gapdh* and their respective paired uninfected controls. (**C**) Dotplots show the alterations of *Mgl2*, *Nos2* and *Arg1* mRNA expression levels due to (co-)infection. (**D**) Dotplots illustrate distinct patterns of chemokine and cytokine mRNA production by macrophages after (co-)infection. (**E**) Dotplots demonstrate (co-)infection induced protein production of chemokines and cytokines that were measured in cell culture supernatants. Dashed lines represent control cultures. *$p < 0.05$, **$p < 0.01$, ***$p < 0.001$, Dunn's test or Tukey HSD test with p-value adjustments for multiple comparisons (Bonferroni-Holm method). $^{\#}p < 0.05$, $^{\#\#}p < 0.01$, $^{\#\#\#}p < 0.001$, Wilcoxon signed-rank test or one-sample t-test for the comparison to uninfected cultures ($\mu = 1$).

925 # Tables

926 **Table I.** Frequencies of blood agar cultures from endpoint blood smears and synovial knee joint swabs positive for
927 β-hemolytic bacteria.

positive cultures	GAS	GAS+IAV	IAV+GAS
blood	20% (2/10)	30% (3/10)	50% (5/10)
knee joint capsule	10% (1/10)	30% (3/10)	50% (5/10)

928 $p = 0.25$, Fisher's exact test